Journal of Solid State Chemistry 184 (2011) 1622–1630

Contents lists available at ScienceDirect

Journal of Solid State Chemistry

journal homepage: www.elsevier.com/locate/jssc

Ab-initio crystal structure prediction. A case study: $NaBH_4$

Riccarda Caputo [a,*], Adem Tekin [b,*]

[a] ETH Zürich, Department of Chemistry and Applied Biosciences, Laboratory of Inorganic Chemistry, Wolfgang-Pauli Str 10, CH-8093 Zürich, Switzerland
[b] Informatics Institute, Istanbul Technical University, 34469 Maslak, Istanbul, Turkey

ARTICLE INFO

Article history:
Received 7 March 2011
Received in revised form
29 April 2011
Accepted 2 May 2011
Available online 7 May 2011

Keywords:
$NaBH_4$
Crystal structure prediction
Global optimizations
Simulated annealing
Density functional theory

ABSTRACT

Crystal structure prediction from first principles is still one of the most challenging and interesting issue in condensed matter science. we explored the potential energy surface of $NaBH_4$ by a combined ab-initio approach, based on global structure optimizations and quantum chemistry. In particular, we used simulated annealing (SA) and density functional theory (DFT) calculations. The methodology enabled the identification of several local minima, of which the global minimum corresponded to the tetragonal ground-state structure ($P4_2/nmc$), and the prediction of higher energy stable structures, among them a monoclinic (Pm) one was identified to be 22.75 kJ/mol above the ground-state at $T=298$ K. In between, orthorhombic and cubic structures were recovered, in particular those with $Pnma$ and $F\bar{4}3m$ symmetries.

1. Introduction

The prediction of crystal structures from completely first-principles approach and using minimal information about bonds and molecular arrangements has been always one of the major issue in crystallography as well as in computational materials science and solid state theory. The question whether crystal structures are in principle predictable is a long-lasting problem that has caught attention for decades [1,2]. Recently, and thanks to an increasing computational power and even more accurate first-principles minimization techniques, the structure prediction has become a very fast growing field of research. Without the knowledge of any experimental information about the structure, the theoretical first-principles approach aims at exploring the potential energy surface of a solid compound and hence determining not only the global minimum, but also any other local minima, which might be adopted. The comparison with known experimental structures helps to validate the predictability power of such an approach and provides a molecular insight of stable and metastable structures of chemical systems. Our approach, we present in this study, to structure prediction involves different stages. In a very general way, and in cases where anything is known about a particular chemical compound, the first step is represented by any plausible and expected chemistry provided by inspecting the stoichiometry of the specific atoms forming the compound. The cluster model built on the chemistry considerations is optimized by using quantum chemistry wave-function methods. The bond lengths and derived specific molecular arrangements provide the minimal structural information for global structure optimizations. By using simulated annealing method as a global optimizer, several configurations are generated and selected ones are subsequently considered in the periodic lattice calculations. Depending on the particular system, the criteria of choice is based on chemical considerations and in particular on the expected low energy configurations forseen by the cluster models. In fact, the quantitative descriptors of crystal geometry are mainly dictated by the strength and directionality of the interatomic forces. Clearly, they represent only the basic factors that determine the crystal structures, being the lattice periodicity the other major factor. An example, reported by the authors, is $LiBH_4$: the cluster model predicted the tridentate configuration as the lowest energy structure, while the periodic lattice calculations showed that actually in the crystal the $[Li]^{\delta+}$ and $[BH_4]^{\delta-}$ units are found in a mixed bi- and tridentate configurations. Following the study of $LiBH_4$ structure [17], we employed the same approach to search for the ground-state and high-lying local minima of $NaBH_4$.

One of the first experimental study of $NaBH_4$ structure was reported by Soldate [3], who determined a face-centered lattice with $a=6.151$ Å, boron–sodium distance of 3.07 Å and boron–boron distance of 4.35 Å. Interestingly, he concluded that the uncertainties of hydrogen position assignment did not allow to get the exact arrangement of $[BH_4]^{\delta-}$ tetrahedron. In addition, the boron–boron distances resulted "*large enough to cause very little*

* Corresponding authors. Fax: + 41 4 46 32 11 49; fax: +90 21 22 85 70 73.
E-mail addresses: riccarda.caputo@inorg.chem.ethz.ch (R. Caputo), adem.tekin@be.itu.edu.tr (A. Tekin).

0022-4596/$ - see front matter © 2011 Elsevier Inc. All rights reserved.
doi:10.1016/j.jssc.2011.05.006

steric hindrance to rotational displacements of $[BH_4]^{\delta-}$ *tetrahedra. Thus, rotating or oscillating* $[BH_4]^{\delta-}$ *tetrahedra can be reasonably presumed to exist in the structure and statistical distributions of tetrahedra, such as the one already considered, are of relevance*" [3]. This issue is the crucial concern we considered in the present work in order to search for other possible stable symmetries that $NaBH_4$ may adopt. The recent study of Kumar et al. [4] confirmed Soldate's results by finding a similar cubic ($Fm3m$) crystal structure for $NaBH_4$ with $a=6.1506$ Å at ambient conditions.

In this structure, each $[BH_4]^{\delta-}$ group is surrounded by six Na atoms and each Na atom by six $[BH_4]^{\delta-}$ groups both in octahedral configuration. It has been shown [4,5] that under the pressure, the crystal structure can transform. More specifically, Kumar et al. [4] and Kim et al. [5] found that the cubic phase is stable up to 5.4 GPa by synchrotron X-ray diffraction. They observed the first phase transition occurring at 6.3 GPa into the tetragonal ($P42_1c$) structure with cell dimensions $a=4.0864$ Å, $c=5.5966$ Å. This phase was first reported by Fischer et al. [6] by neutron diffraction at 10 K with cell dimensions $a=4.333$ Å, $c=5.869$ Å. At 8.9 GPa another transition to orthorhombic ($Pnma$) phase was found with cell dimensions $a=7.3890$ Å, $b=4.1660$ Å, $c=5.6334$ Å. Under 30 GPa pressure, orthorhombic phase remained stable. Synchrotron powder diffraction study of Filinchuk et al. [7] confirmed the high-pressure findings of Kumar et al. [4] and Kim et al. [5] by observing phase transitions near 6 and 8 GPa into the $P42_1c$ and $Pnma$ phases, respectively. In $P42_1c$ and $Pnma$ phases, $[Na]^{\delta+}$ atoms and $[BH_4]^{\delta-}$ groups are in distorted octahedral coordination. In addition to these phases, Fischer et al. [8] reported another tetragonal ($P4_2/nmc$) low temperature structure by means of powder neutron diffraction. At 10 K the lattice parameters of ($P4_2/nmc$) phase are $a=4.332$ Å, $c=5.869$ Å, which are quite in agreement with the lattice parameters obtained from an early X-ray diffraction study at 78 K [9]. ($P4_2/nmc$) phase was also found to be the low temperature structure for KBH_4 with both X-ray powder and neutron diffraction methods [10]. Phase transitions in $NaBH_4$ are motivated by order–disorder preference of mobile $[BH_4]^{\delta-}$ groups, e.g., the transition from the disordered high temperature phase ($Fm3m$) to the ordered low temperature phase ($P42_1c$) occurs at 190 K [10].

In addition to the neutron and X-ray experiments, theoretical studies have also been performed to find the ground-state crystal structure of $NaBH_4$. The projected-augmented plane-wave calculations of Vajeeston et al. [11] predicted that at low temperature $NaBH_4$ crystallizes into the tetragonal $P4_2/nmc$ structure, with cell dimensions ($a=4.3452$ Å, $c=5.8597$ Å) which are quite in agreement with the experimental results of Fischer et al. [8], rather than the tetragonal $P42_1c$ phase. In particular, they obtained the $P4_2/nmc$ structure lower in energy than the $P42_1c$ and $Fm3m$ by only 5.6 and 27 MeV, respectively. More recently, Kim et al. [5] considered $Fm3m$, $P42_1c$ and $Pnma$ phases of $NaBH_4$ in Car–Parrinello molecular dynamics simulations. They found the tetragonal ($P42_1c$) phase energetically favorable at zero temperature and pressure with cell dimensions lower than that of Fischer et al. [8] by % 2–3. However, at finite temperatures, the cubic ($Fm3m$) phase was obtained lower in energy than the tetragonal phase. The phase diagram studies have been recently reported [4,5,12–15]. Nevertheless, the discrepancy between the experimental results and a missing theoretical study considering all the phases mentioned above from first-principles urged us to perform an unbiased structural search based on simulated annealing (SA) [16] aiming to find the ground-state structure of $NaBH_4$, following the same approach applied for $LiBH_4$ [17] and $Mg(BH_4)_2$ [18]. The resulting structures from the SA global optimizations as well as the experimental ones were further treated by high accurate plane wave density functional theory (DFT) calculations.

2. Computational methods

We first modelled a cluster to elucidate the energetically most favorable configurations in a one formula unit of $NaBH_4$. We calculated the all-electron total energy as a function of Na–B distance by using DMol3 code as implemented in Materials Studio 5.0. In particular, we used the DFT approach and GGA PBE for the exchange-correlation functional with a triple numerical plus polarization (TNP) basis set. The orbital cutoff, the SCF tolerance ($1.0e^{-6}$ Ry) and the multipole expansion (octupole) were set up in order to achieve the best convergency.

For the periodic lattice calculations, we employed DFT-based methods, in particular, Quantum Espresso [19] and CASTEP [20], implemented in Materials Studio 5.0. The former code was used as a counter-check of the structures optimized by using CASTEP and to validate the lattice stability by performing phonon calculations. In CASTEP, we used Norm-conserving pseudopotentials for all atoms and a fine mesh of k points, which depended on the specific lattice dimensions. The energy conversion threshold was set to 0.01 MeV/atom, with maximum displacement of 0.001 Å and maximum force of 0.001 eV/Å, yielding a high accuracy for the energy and atomic displacements. For sodium and boron atoms the valence region was modelled using the $3s^1$ and $2s^22p^1$ electrons, respectively. The Perdew–Burke–Ernzerhof 96 and the generalized gradient form (GGA-PBE) of the exchange-correlation functional were applied. Density functional perturbation theory (DFPT) as implemented in CASTEP [21,22] was used for phonon calculations. The simulated infrared (IR) spectra were calculated using the property analysis implemented in Materials Studio 5.0. Furthermore, the Reflex powder diffraction module, implemented in Materials Studio 5.0, was used to simulate the XRD patterns of the optimized structures. In the simulations, we used the X-ray radiation with Cu source and $\lambda_1 = 1.5405$ Å. In Quantum Espresso, we employed variable cell calculations for relaxing the lattice of the structures optimized with CASTEP. PW91 ultra-soft pseudopotentials were used with nine and three electrons representing the valence shell of Na and B atoms, respectively. The kinetic energy cutoff (Ry) of wavefunctions was set to 60 Ry, equivalent to 816.34 eV. The DFTP phonon calculations were employed to ascertain the lattice stability and make a counter-check of the phonon dispersion curve obtained by CASTEP.

In order to scan the potential energy surface (PES) of $NaBH_4$, we employed a crystal structure prediction method based on SA which has been successfully applied to $Mg(BH_4)_2$ [18], $Mg(NH_3)_nCl_2$ [23] with $n=6$, 2, 1 and $LiBH_4$ [17]. As we discussed in [18,17], the number of bonds between metal (M) and hydrogen (H) atoms represents one of the key parameters that stabilize crystal structures. This fact was also considered for $NaBH_4$. Accordingly, we constructed the crystal structures by maximizing the number of Na–H bonds within $(2\times2\times2)$ cut-through lattice using only bond length constraints and one, two and four formula unit (f.u.) similar to the $LiBH_4$ [17] case. A representative model and its details can be found elsewhere [17]. The only difference from the $LiBH_4$ model is the employment of new bond distance thresholds and the distances used in the fitness function. All these distances were initially taken from the crystal structure built on the cluster model. In particular, if the Na–B, Na–Na, B–B, and H–H distances in the $(2\times2\times2)$ cut-through lattice were longer than 2.24, 3.77, 3.78, and 2.3 Å, respectively, then the resultant crystal structure was accepted as a potential candidate. Besides this distance threshold set, the following one was also used: 2.93, 4.2, 4.2, 2.3 Å. The fitness criteria in SA optimizations, namely the total number of Na–H bonds in the cut-through lattice, were determined by simply counting the number of bonds, for one the following three different Na–H bond ranges: (2.38, 2.73) Å (2.44, 2.48) Å and (2.45, 2.65) Å. By varying the Na–H distance

range, it was possible to map the PES of $NaBH_4$. The best promising structures were then further treated by CASTEP and Quantum Espresso.

3. Results and discussion

3.1. Structure

The initial cluster model was designed by using one formula unit of $NaBH_4$ [24]. We first optimized the coordinates of the isolated $NaBH_4$ molecule in order to get the boron–hydrogen bond lengths. Then keeping the coordinates of the (BH_4) unit we calculated the total energy as a function of the sodium–boron distance in the three geometrically non-equivalent configurations, namely tridenate, bidentate and monodenate. We employed all-electron wave-function calculations at unrestricted Hartree–Fock (UHF) and second-order Møller–Plesset perturbation (MP2) theory to search for the minimum energy distance between sodium and boron atoms for these three configurations, in addition to DMOL3 calculations. At all levels of theory, the bidentate and tridentate configurations resulted very close in energy, indicating that a slight rotation of $[BH_4]^{\delta-}$ unit is possible. In all cases, the tridentate resulted as the lowest energy configuration, supporting the findings of Francisco et al. [25]. Clearly, the tridentate configuration enables the shortest Na–B distance while the monodentate pushes further the sodium atoms being collinear with hydrogen. In fact, the Na–B distance increased from 2.299 Å in the tridentate configuration to 3.000 Å in the monodentate configuration. The energy difference between the bidentate and tridentate configurations resulted 19.60 kJ/mol by using DMol3. This is the maximum energy difference we can expect in a lattice where the symmetry allows a pure bidentate or a pure tridentate arrangement of a $[Na]^{\delta+}$ and $[BH_4]^{\delta-}$ ions to each other. Fig. 1 shows the total all-electron energy as a function of Na–B distance of the three non-equivalent configurations calculated by DMol3.

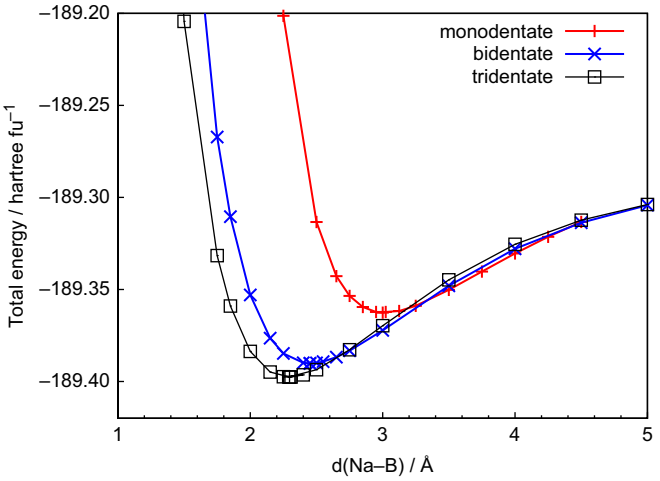

Fig. 1. The total all-electron energy as a function of Na–B distance of the three non-equivalent configurations: monodentate, bidentate and tridentate. All electron total energies were calculated by using DMol3.

Both bidentate and tridentate configurations were used to build the periodic lattice. The tridentate configuration resulted in a periodic lattice characterized by a distorted bidentate–tridentate configuration with no symmetry up to a tolerance of 0.01 Å of the atomic positions. On the other hand, the employment of the bidentate structure consisting of two formula units converged to a tetragonal $P4_2/nmc$ symmetry (IT 137), which is characterized by the bidentate configuration. Then, the bond distances needed for the SA global structure optimizations were extracted from this model structure. The SA method yielded many distinct structures for $NaBH_4$ having different number of Na–H coordinations. Twenty two of them were selected for the subsequent periodic DFT calculations. Three of them converged to the lowest energy structure with symmetry group $P4_2/nmc$ (IT 137). The two tetragonal structures with symmetry groups 137 and 114 differed in terms of an energy by 6.01 kJ/mol. That difference was larger than the data reported in [6,8]. The two symmetry groups differ in the number of symmetry operations, which are double in the group 137, exactly 16 instead of eight in the group 114. The symmetry group 114 is in fact one of the maximal non-isomorphic subgroup of the symmetry group 137. Interestingly, the lowest energy tetragonal structure is characterized by a perfectly bidentate configuration of sodium atoms, which occupy the half-edge and face center of the conventional unit cell. Fig. 2 shows a 3D-view of the tetragonal (IT 137) and monoclinic (IT 6) structures

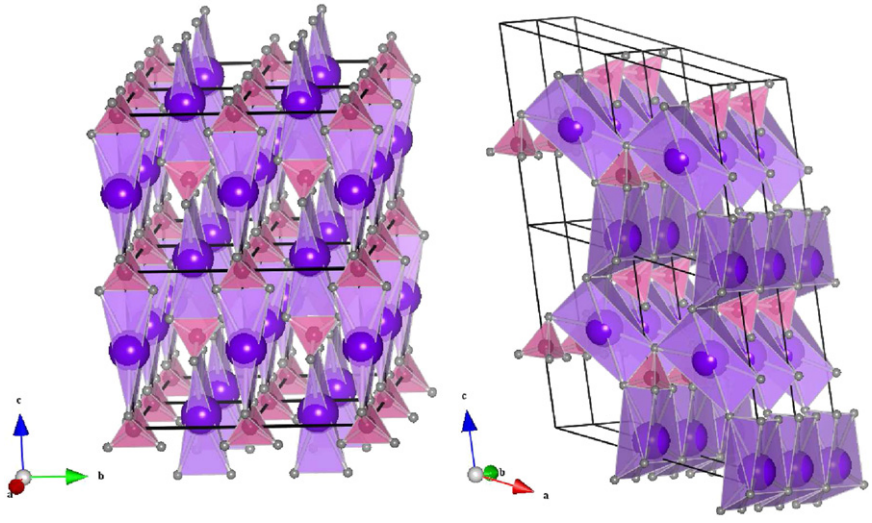

Fig. 2. A 3D-view of the lowest (tetragonal IT 137) and highest (monoclinic IT 6) structures. The polyhedral representation of the Na atom bonds highlight the perfect bidentate configuration in the former structure and a mixed bi- and tridenate in the latter structure. Representing color: Na, violet; B, pink; H, gray. (For interpretation of the references to color in this figure legend, the reader is referred to the web version of this article.)

and Tables 1 and 2 list the Wyckoff positions of these structures, respectively.

Among the highest energy structures, the monoclinic one was found to be stable with 17.53 kJ/mol above the tetragonal (IT 114) structure and 23.55 kJ/mol above the ground-state tetragonal (IT 137). This difference reduced to 16.51 and 22.51 kJ/mol when the zero-point energies were considered, respectively. We also modelled the hexagonal structure with $P6_3mc$ symmetry proposed by Soulié et al. [26] as a high temperature phase of $LiBH_4$. Similar to $LiBH_4$ case [17], this structure was found to be unstable due to the existence of imaginary modes in the phonon calculations.

Between these two extreme cases, other stable structures were found with orthorhombic, cubic and tetragonal symmetries. In particular, by our approach we obtained the orthorhombic structure already reported by Filinchuk and co-workers [7] as the high pressure γ-$NaBH_4$ phase with *Pnma* (IT 62) symmetry. It resulted only 1.01 and 7.02 kJ/mol above the tetragonal structures, respectively, IT 114 and IT 137, but almost isoenergetic (by only 0.08 kJ/mol) with the structure optimized starting from the Ref. [7].

The very small energy difference between the tetragonal and the orthorhombic *Pnma* structures are clearly rationalized by considering the rotational degree of freedom of the $[BH_4]^{\delta-}$ group in the lattice. In fact, while the $[BH_4]^{\delta-}$ groups are all eclipsed in the tetragonal structure, they are staggered along the *b*-direction in the orthorhombic structure.

Another stable orthorhombic structure with symmetry group $Pnm2_1$ (IT 31) found by the SA search, 5.43 kJ/mol above the tetragonal IT 114, shows a completely different coordination of sodium atoms. More specifically, they are surrounded by four $[BH_4]^{\delta-}$ groups in a tridentate and bidentate coordinations as shown in Fig. 3. In addition, they differed in the molar volume, being larger of the higher energy structure by 11.84 $Å^3\ mol^{-1}$. Amongst the cubic structures, the face centered one with $F\bar{4}3m$ (IT 216) symmetry, generally reported as the stable room-temperature structure [6,8] was found to be 5.89 kJ/mol higher in energy than the tetragonal IT 114 structure and 11.90 kJ/mol above the ground-state and almost isoenergetic to the orthorhombic $Pnm2_1$ structure: they differ by only 0.46 kJ/mol. When the zero-point energies were considered, the $F\bar{4}m$ structure differs from the ground-state by 8.78 kJ/mol. The face centered cubic structure can be seen as a sodium fcc lattice in which the octahedral sites are occupied by $[BH_4]^{\delta-}$ groups, oriented in a bidentate way to sodium atoms and eclipsed to each other, as shown in Fig. 3. Besides the $F\bar{4}3m$ phase, another almost isoenergetic cubic structure with $P2_13$ (IT 198) symmetry, was found to be stable, 5.84 and 11.85 kJ/mol above the tetragonal structures, respectively, IT 114 and IT 137. The reduced number of symmetry operations in the last cubic structure, 12 compared to 96 in the fcc structure, is due to the local configuration of $[BH_4]^{\delta-}$ groups, which rearrange almost tridentate towards the sodium atoms and eclipsed to each other when the structure is projected along the crystallographic axes. The two cubic structures differed only in a slight rotation of the $[BH_4]^{\delta-}$ groups.

Table 1
The Wyckoff positions of the tetragonal lowest energy structure with symmetry group $P4_2/nmc$ (IT 137) and lattice parameters 4.357 Å, 4.357 Å, 5.902 Å.

Atom	*x*	*y*	*z*	Site
Na	0	0	0.5	2*b*
B	0	0	0	2*a*
H	0	−0.22868	0.88196	8*g*

Table 2
The Wyckoff positions of the monoclinic highest energy structure with symmetry group *Pm* (IT 6) and lattice parameters 4.674 Å, 4.409 Å, 8.184 Å, $\beta = 113.340°$.

Atom	*x*	*y*	*z*	Site
H	0.61718	0.71834	0.84080	2*c*
H	0.11964	0.22811	0.36166	2*c*
Na	0.92372	0	0.07751	1*a*
Na	0.61911	0	0.58744	1*a*
B	0.01440	0	0.40149	1*a*
H	0.08935	0	0.56150	1*a*
H	0.73116	0	0.32171	1*a*
B	0.78103	0.5	0.84849	1*b*
H	0.01456	0.5	0.98733	1*b*
H	0.86502	0.5	0.72562	1*b*

3.2. X-ray diffraction pattern

Soldate [3] reported 20 diffraction peaks for the face-centered structure with lattice parameter 6.151 Å. Our calculated XRD patterns for both cubic structures perfectly reproduce Soldate's data with an exception that the $P2_13$ phase has faint intensity peaks, which are not present in the face centered cubic structure as shown in Fig. 4. For all the stable structures, significant differences of diffraction peaks were obtained in the range of 2θ (25,30)°. The most intense peaks of the cubic $F\bar{4}3m$ and $P2_13$ phases were located at 28.79 and 29.04°, respectively, due to the slightly upwards shift of the (2 0 0) plane. In the tetragonal structure (IT 137) the most intense diffraction peak is due to the (110) plane at 28.96°, while the diffraction of the (0 0 2) plane falls at 30.27° with less intensity. The diffraction of the (1 1 1) plane of the face centered cubic structure at 24.86° is replaced by the diffraction of (1 0 1) plane at 25.40° in the tetragonal structure. A complete comparison of the diffraction peaks are shown in Fig. 4. The different coordination of sodium atoms in the two stable orthorhombic structures is clearly reflected in the corresponding diffraction patterns. The less symmetry operations (4) in the $Pnm2_1$ structure compared to the *Pnma* one (8) brings additional peaks, which are not present in the diffraction pattern of the more symmetric structure as shown in Fig. 4.

3.3. Enthalpy of formation

The enthalpy of formation was calculated as the energy difference between the total energies of the specific $NaBH_4$ structure and the sum of the total energies of Na, B and H_2, which were previously optimized [27,28]. In agreement with other authors, as mentioned in the introduction section, and as reported elsewhere [28–30] the face centered structure of $NaBH_4$ is not the ground-state structure, instead the tetragonal structure has been already reported as the low temperature structure. The present first-principles study confirmed that it is effectively the ground-state structure. To ascertain the consistency of the energy trend along the optimized stable structures, we counterchecked the total energy calculations by using Quantum Espresso in parallel to CASTEP. The optimized geometries obtained from CASTEP were used as initial geometries in Quantum Espresso optimizations. The two codes gave consistently the same trend even if the corresponding total energy constantly differed by a quantity depending on the specific optimization algorithms and pseudopotentials used.

In Table 3, we report the calculated enthalpies of formation of $NaBH_4$ together with structural data calculated by using CASTEP. The thermal contribution to the enthalpy of formation was accounted by the numerical integration over temperature, up to 298 K, of the heat capacity, which was derived from phonon dispersion calculations, as reported in [31,17]. Interestingly, the

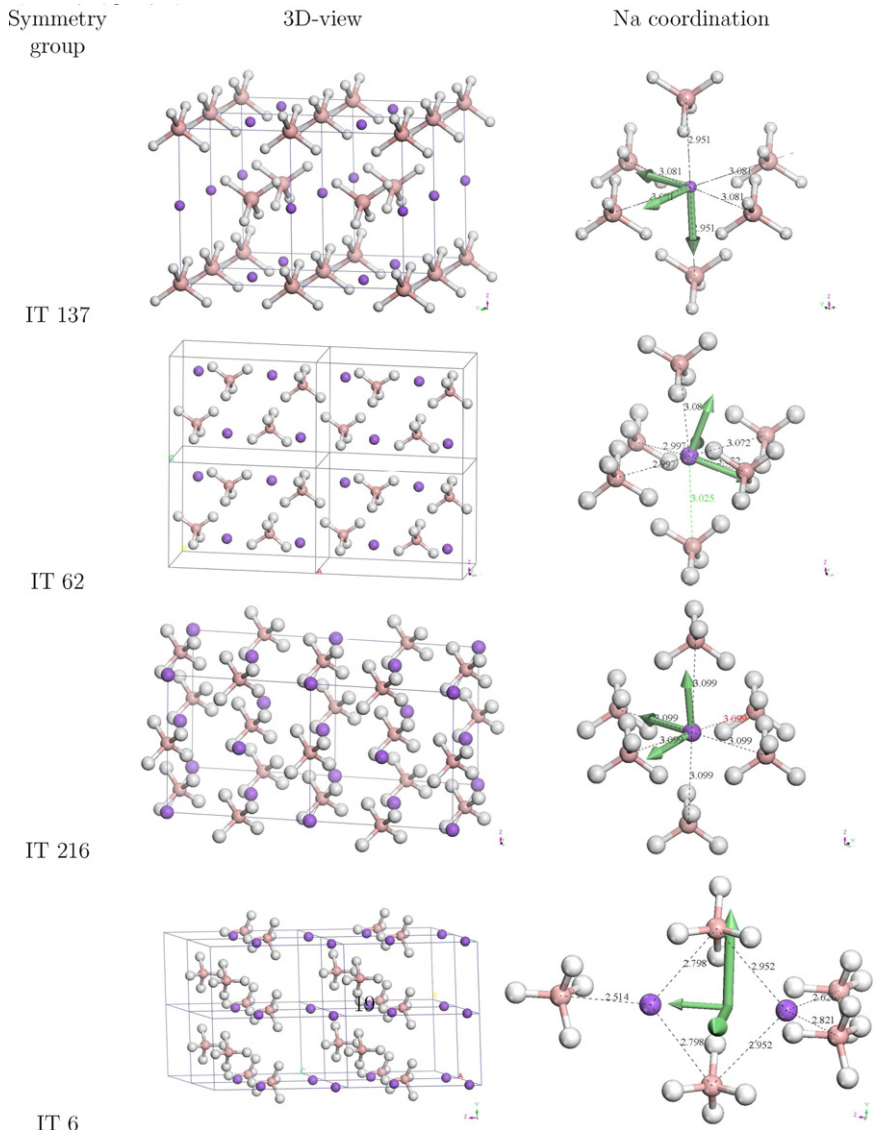

Fig. 3. The Na coordination. A view of the nearest neighbor $[BH_4]^{\delta-}$ groups to $[Na]^{\delta+}$ and a 3D view of the corresponding periodic conventional cells. Representing color: Na, violet; B, pink; H, white. (For interpretation of the references to color in this figure legend, the reader is referred to the web version of this article.)

structure reported in [29], obtained after the full geometry optimization of one of our SA models, assumed the tetragonal symmetry (IT 137) by a very slight change of the lattice angles: 89.9877, 90.0070, 90.0029° which become 90.00°, as required by the tetragonal symmetry by searching for the best interpolating symmetry. The maximum deviation of the interpolated atomic positions from the optimized atomic positions was only 0.02 Å. The energy difference between the as-optimized triclinic structure and the tetragonal structure with IT 114 was only 6.01 kJ/mol. We comment on that structure because it represents an example of how the alignment of the $[BH_4]^{\delta-}$–Na-$[BH_4]^{\delta-}$ fragment and hence *C*2 axis respect to the crystallographic *b*-axis can affect the symmetry group and the total energy. Phonon calculations, discussed in the next section, were used to evaluate the temperature dependence of the energy and lattice heat capacity in a quasi-harmonic approximation [21]. These results can be directly compared with heat capacity measurements, for instance to predict the relative phase stability of different structural modifications. The zero-point energy contribution did not change the energy differences between the proposed stable high energy (monoclinic IT 6) structure and the face centered cubic (IT 216) structure: the energy differences resulted 11.64 and 13.73 kJ/mol, without and with the zero-point energy, respectively. The heat capacity of $NaBH_4$ was already determined by Boodman and a couple of years later by [32] (and references therein). They found that a second-order transition occurred at 189.9 K. We calculated the heat capacity of four representing structures of each crystal family via numerical integration of the phonon dispersion curve [21], as shown in Fig. 5. A general agreement was found with the one of the first experimental results [32]. In particular, the heat capacity of the cubic fcc structure, which is higher at lower temperatures, becomes lower with increasing temperature and intersects the heat capacities of the tetragonal (IT 137) and the monoclinic (IT 6) structures at 182.5 and 190.0 K, respectively. Clearly, this is the temperature range where the phase transition is expected. The thermal contribution to the enthalpies did not change the energy order of the different stable structures.

In Table 4, the zero-point energy and the thermal contribution of the four representative structures are reported. Considering, for example the tetragonal IT 137 structure and the proposed monoclinic structure IT 6, the enthalpy difference at $T = 298$ K becomes 22.75 kJ/mol, compared to 23.55 and 22.51 kJ/mol without and with including the zero-point energy, respectively. Moreover, the

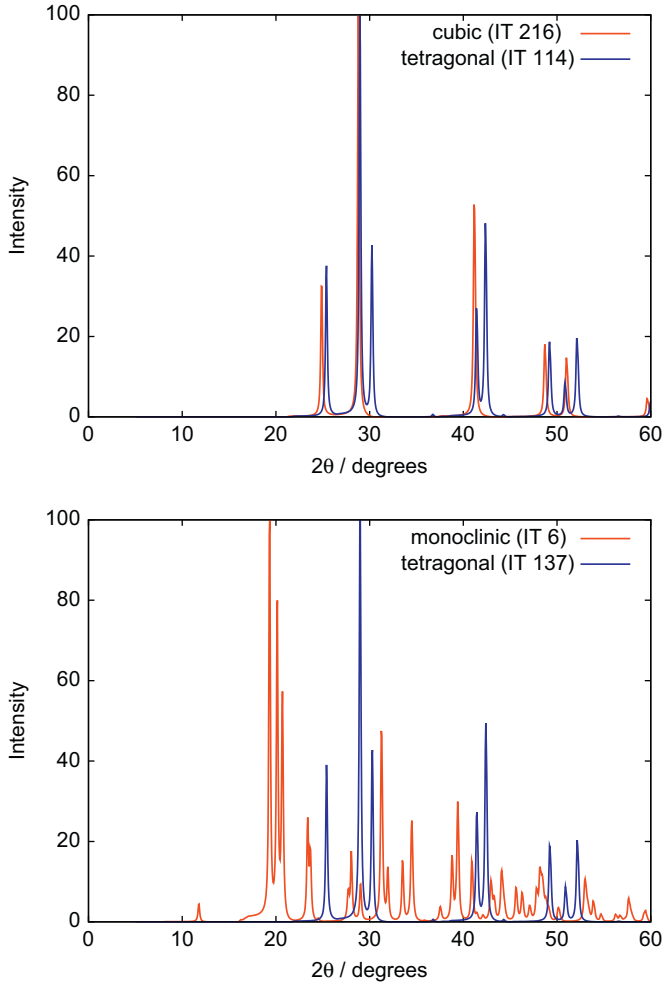

Fig. 4. The calculated XRD patterns of the face centered cubic (IT 216) and the tetragonal (IT 114) are compared with the highest and the lowest energy structures, the monoclinic (IT 6) and the tetragonal (IT 137), respectively. The most intense peak of the cubic structure (2 0 0) at 28.78° is split in two peaks (1 1 0) and (0 0 2) at 28.94° and 30.30°, respectively, in the tetragonal structure. Similarly, the single peak (2 2 0) at 41.26° of the cubic structure falls in the range of diffraction of (2 0 2) and (1 1 2) planes of the tetragonal. The most intense peaks of the monoclinic structure are shifted to lower diffraction angles. In particular, three diffractions in the range of 20° are present: (1 0 $\bar{1}$), (0 1 0) and (1 0 0) at 19.31°, 20.12° and 20.73°, respectively.

tetragonal IT 114 differed from the monoclinic structure by 17.549, 16.585 and 16.71 kJ/mol, without, with the zero-point energy and considering the thermal contribution, respectively. Interestingly, the value reported by [32], $(H-H_o)$ is 3890.1 cal/mol, which is 16.28 kJ/mol. If we attribute the energy difference between the cubic (IT 216) and the tetragonal (IT 137) to an applied external pressure (isobaric stress) then a rough estimation of the pressure required to promote the transition is 11.453 GPa at $T = 298$ K. Similarly, the transition at $T = 0$ K from the tetragonal IT 137 to the monoclinic IT 6 structure will require a pressure of 1.753 GPa, included the zero-point energy. That might indicate that the

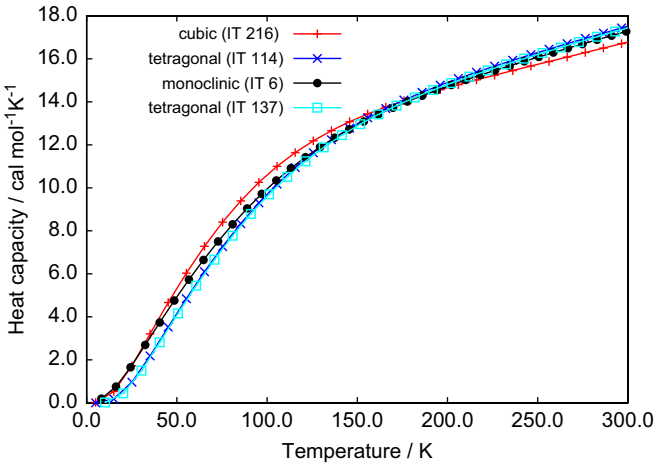

Fig. 5. The heat capacity of four representative structures. It was calculated via numerical integration of the phonon dispersion curves.

Table 4
The enthalpies of formation of four representative structures calculated by including the zero-point energy and the thermal contribution up to T=298 K.

Symmetry group	$\Delta_f H_{(ZPE)}(0)$	$\Delta_f H(298)$
$P4_2/nmc$ (137)	−256.225	−265.249
$P\bar{4}2_1c$ (114)	−250.298	−259.210
$F\bar{4}3\,m$ (IT 216)	−247.442	−256.087
Pm (6)	−233.712	−242.504

Table 3
Structural and thermodynamic data of the stable structures found by using the combined ab-initio geometry optimization approach. The last column reports the max deviation of the optimized Cartesian coordinates from the lattice positions represented by the corresponding symmetry. The lowest and highest energy structures adopt a tetragonal and a monoclinic symmetry, respectively. The hexagonal structure, which has lattice instability, is reported here for a mere comparison.

Crystal family	$\Delta_f H_0$ (kJ/mol)	a, b, c (Å), β (deg)	Symmetry group (IT)	Molar volume (cm^3/mol)	Mass density (g/cm^3)	Max deviation (Å)
Tetragonal	−257.83	4.357, 4.357, 5.902	$P4_2/nmc$ (137)	33.785	1.12	0.0001
	−251.82	4.359, 4.359, 5.909	$P\bar{4}2_1c$ (114)	33.741	1.12	0.001
	−251.65	6.01	$I4_1/acd$ (IT 142)	33.775	1.120	0.039
	−248.90	6.163, 6.163, 6.024	$P\bar{4}$ (81)	34.444	1.10	0.0001
	−247.82	7.605, 7.605, 4.512	$P4_2/m$ (84)	39.289	0.96	0.0001
Orthorhombic	−255.38	4.79, 7.51, 8.57	$P2_12_12_1$ (IT 19)	46.421	0.815	0.0409
	−250.81	8.435, 4.362, 6.101	$Pnma$ (IT 62)	33.797	1.12	0.0001
	−246.39	4.812, 7.166, 7.884	$Pmn2_1$ (IT 31)	40.929	0.924	0.0001
Cubic	−245.98	6.156	$P2_13$ (IT 198)	35.120	1.077	0.0001
	−245.93	6.124	$F\bar{4}3m$ (IT 216)	34.585	1.094	0.0001
Monoclinic	−234.28	4.674, 4.409, 8.184 113.340	Pm (6)	46.631	0.811	0.0001
Hexagonal	−238.71	4.687, 4.687, 8.117	$P6_3mc$ (186)	46.510	0.813	0.001

monoclinic high energy structure is a local minimum between two more stable or better experimentally achievable structures. Accordingly, the monoclinic structure might be simply a structural transformation between the tetragonal and the cubic ones.

3.4. Phonon and IR spectra calculations

The phonon calculations helped to discriminate the stable structures. Considering the frequencies of the normal modes of vibration, the two tetragonal structures with symmetry groups 137 and 114 were indistinguishable as shown in Fig. 6. Amongst the two orthorhombic structures, the $Pnm2_1$ one showed two translational imaginary modes out of 72 normal modes. Instead, when the structure adopted the more symmetric configuration *Pnma*, the translational instability was released. Both the two cubic structures with symmetry groups 198 and 216 showed the characteristic modes in the same range of frequencies with very slight differences. The hexagonal structure, modelled similarly to $LiBH_4$ revealed unstability due to the first five imaginary modes out of 36 normal modes of vibrations. The wave numbers obtained by using CASTEP and Quantum Espresso slightly differed. For example, the stretching modes of the tetragonal low energy structure with $P4_2/nmc$ symmetry fall in the ranges $(2323.8,\ 2408.8)\,cm^{-1}$ and $(2330.0,\ 2406.8)$ by using CASTEP and Quantum Espresso, respectively.

In Fig. 7, we compare the calculated IR spectra of the lowest energy tetragonal (IT 137) and highest energy monoclinic (IT 6) structures. The zoomed figure shows a comparison of the stretching modes of the B–H bonds, which are shifted in the highest energy structure compared to the lowest energy structure. In particular, the asymmetric stretching mode at 2350.8 cm^{-1} of the tetragonal structure is split into two active symmetric stretching modes at 2287.8 and 2297.5 cm^{-1} in the monoclinic structure, while the symmetric stretching mode at 2374.3 of the tetragonal structure located at 2387.1 cm^{-1} in the monoclinic structure and it is asymmetric. The monoclinic structure showed four active asymmetric stretching modes in the range of wave numbers $(2330.2,\ 2348.7)\,cm^{-1}$.

3.5. Electronic density of states

As the lattice symmetry is dictated by the local coordination of $[Na]^{\delta+}$ cations to $[BH_4]^{\delta-}$ anions, more precisely by the of type of Na–H coordination (monodentate, bidentate or tridentate) the electronic density of states and hence the orbital energy displacements were slightly affected by the coordination type. What affected the orbital energy alignment was the bond formation, which is always strong, between the boron and hydrogen atoms. As shown in Fig. 8, the low energy states representing the *s* and *p* states of sodium atoms were unaffected by the symmetry and configuration adopted by the specific structure. A separation between those states and the states responsible of the B–H bonds was clearly visible, independently of the particular symmetry adopted by the lattice. The high energy states up to the Fermi level revealed instead a symmetry dependence of the *s*–*p* states of boron and hydrogen atoms. In fact, the states about -6.0 eV describe the electronic states of $[BH_4]^{\delta-}$ groups as a whole whereas those in the range $(-2.0,\ -0.5)$ describe the states of the boron–hydrogen bonds. In that range of energy, the typical alignment of the molecular orbitals of the isolated BH_4^- anion is found only for the face centered cubic structure (IT 216). In fact, as shown in the Fig. 8, the two peaks resemble the a_1 and t_2 states of the isolated BH_4^- anion, with the ratio 1:3. Clearly, the symmetry group, due to the resulting different coordination of $[BH_4]^{\delta-}$ groups to $[Na]^{\delta+}$, affects the separation between the (*s*,*p*) states of the (B–H) bonds. Accordingly, the anionic molecular orbitals are no more aligned as in the isolated tetrahedral.

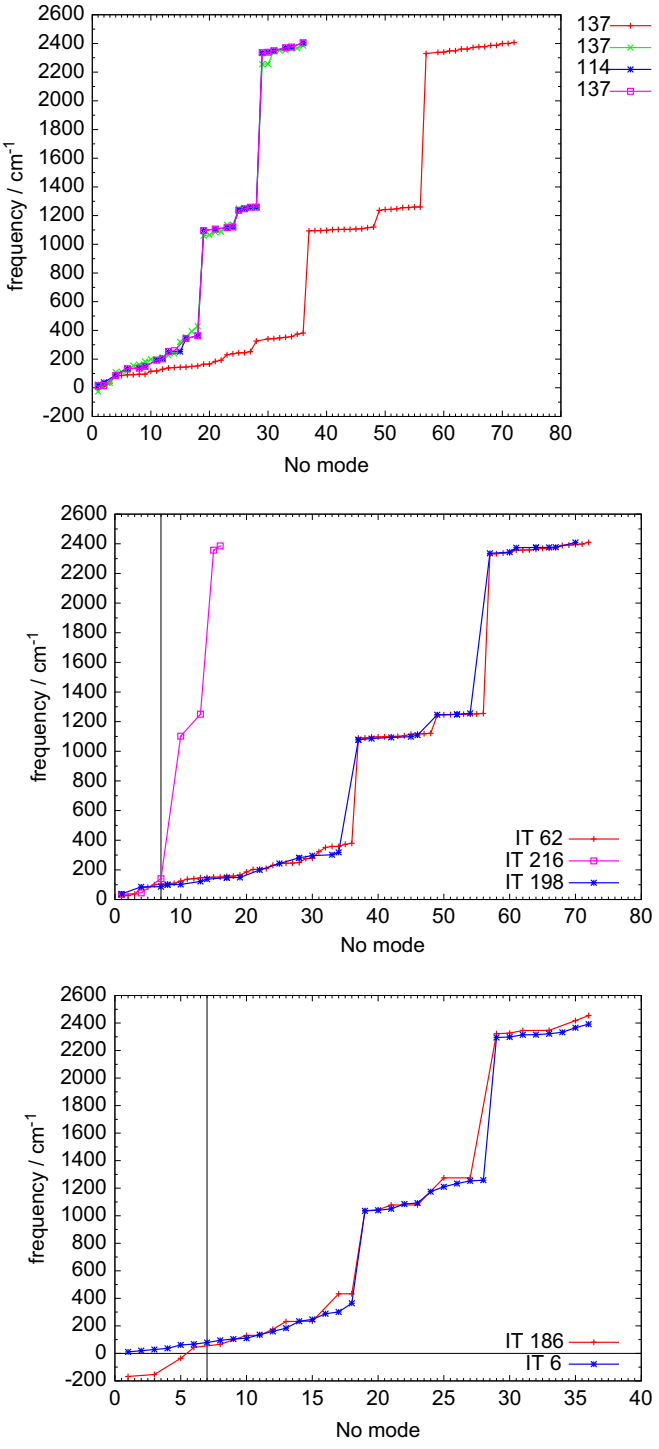

Fig. 6. The calculated frequencies of the normal modes of vibration of representative structures by using Quantum Espresso. The crystal families reported are: (upper panel) tetragonal, (middle panel) orthorhombic and face centered cubic, (bottom panel) monoclinic and hexagonal.

4. Conclusions

In conclusion, we reported the validity of our combined computational approach to explore the potential energy surface and predict stable structures. Our approach, completely from first-principles,

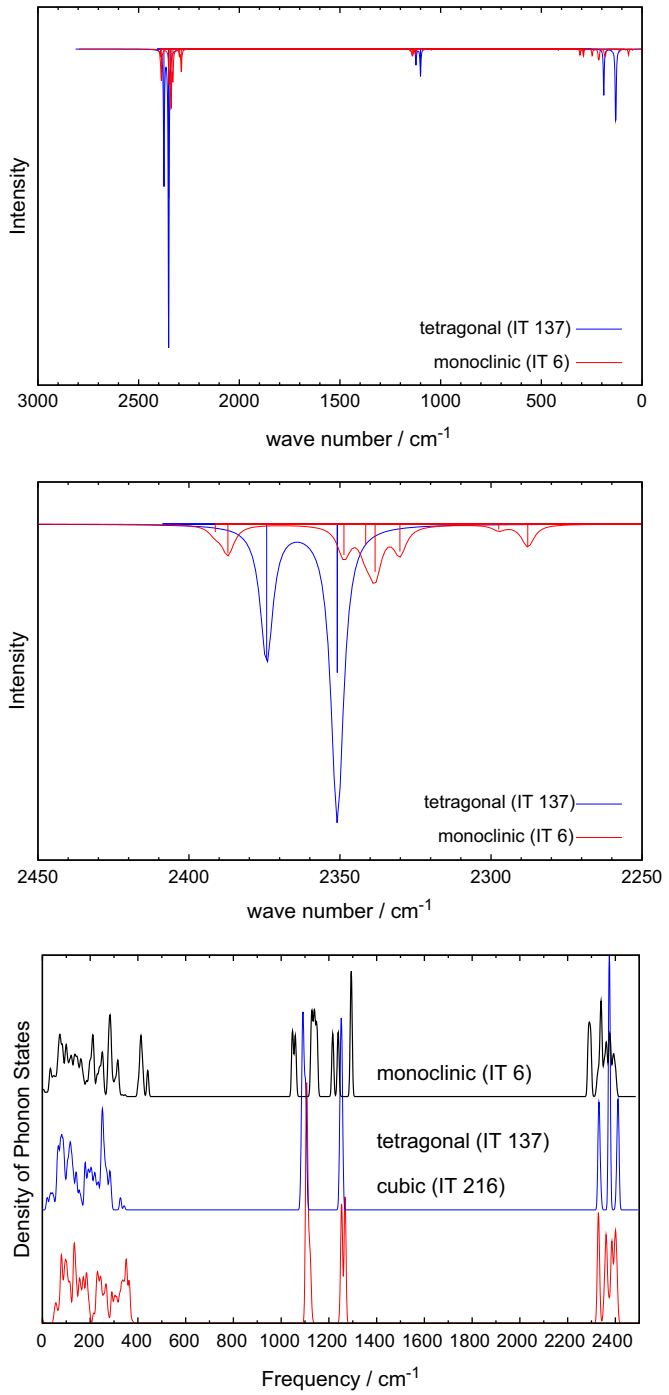

Fig. 7. (up) The calculated IR spectra of the lowest and the highest energy structures with symmetry group tetragonal (IT 137) and monoclinic (IT 6), respectively. (middle) The zoom of the stretching mode region (2330, 2380). (down) The density of phonon states of the lowest (tetragonal), intermediate (cubic) and highest (monoclinic) energy structures, respectively.

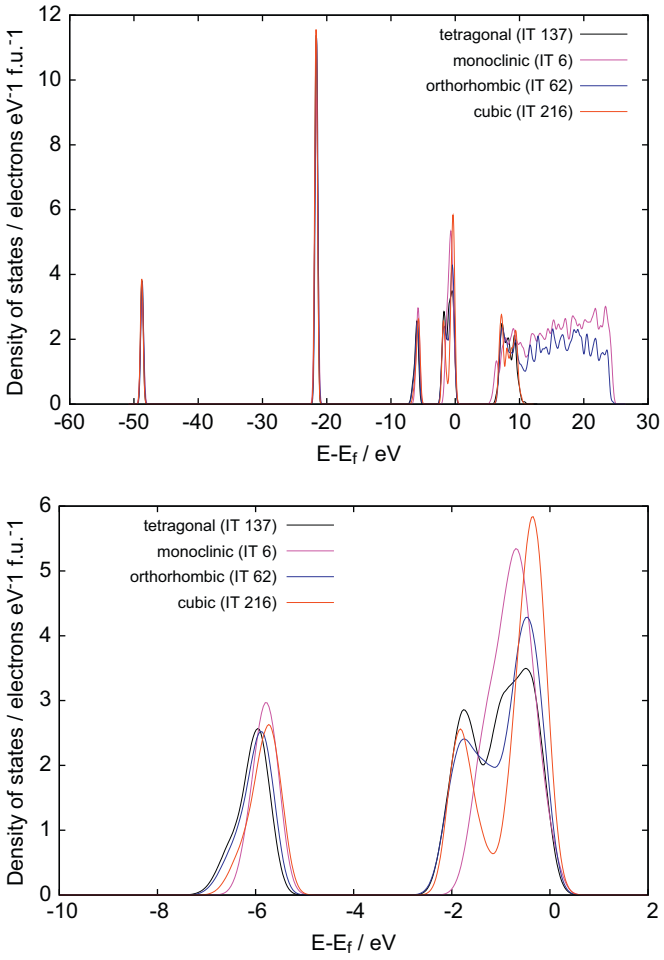

Fig. 8. (up) The total electron density of states of the highest and lowest energy structures, namely the tetragonal (IT 137) and the monoclinic (IT 6) compared with two structures of the other representative symmetry groups, namely orthorhombic (IT 62) and cubic (IT 216). (down) The zoom in the energy range describing the B–H bonds. Only the cubic (IT 216) structure shows the typical states of the isolated BH BH_4^- anion. The other structures, due to a shorter Na–B distance and a different configuration of $[BH_4]^{\delta-}$ groups to $[Na]^{\delta+}$, show a distorted alignment of the orbitals describing the B–H bonds. In the monoclinic structure those state are degenerate.

was able to reproduce known symmetries of $NaBH_4$ and in particular the low energy tetragonal structure and local minimum energy structures, with cubic and orthorhombic symmetry. A stable high energy structure, with monoclinic symmetry was also found. Whether it might be experimentally achievable and identified, the monoclinic high energy structure revealed an interesting Na coordination, which eventually represents either a distinct high energy structure, reachable via thermal energy, or a local minimum between two lower minima, namely the tetragonal and the cubic structures. The phonon calculations helped to confirm the lattice stability of the optimized structures and compare the vibrational frequencies with those already reported in literature [12,5]. Clearly, the present study can reveal thermodynamically stable structures regardless whether they are achievable via thermal energy or external pressure. Accordingly, the high energy structure does not necessarily mean the high temperature structure.

Acknowledgments

We gratefully thank Professor Reinhard Nesper for his valuable comments. The use of linux cluster *Ipazia* at EMPA is greatly appreciated. The Informatics Institute of Istanbul Technical University is acknowledged for computer time and Ozden Akinci for his technical assistance.

References

[1] A. Gavazzotti, Acc. Chem. Res. 27 (1994) 309–314.
[2] S. Woodley, R. Catlow, Nat. Mater. 7 (2008) 937.
[3] A.M. Soldate, J. Am. Chem. Soc. 69 (1947) 987.
[4] R. Kumar, A. Cornelius, Appl. Phys. Lett. 87 (2005) 261916.

[5] E. Kim, R. Kumar, P. Weck, A.L. Cornelius, A. Nicol, S. Vogel, J. Zhang, M. Hartl, A. Stowe, L. Daemen, Y. Zhao, J. Phys. Chem. B 111 (2007) 13873–13876.
[6] P. Fischer, A. Züttel, Order-disorder phase transition in NaBD4, Technical Report, Paul Scherrer Institute, 〈http://num.web.psi.ch/reports/2001/pdf/g09.pdf〉, 2001.
[7] Y. Filinchuk, A.V. Talyzin, D. Chernyshov, V. Dmitriev, Phys. Rev. B. 76 (2007) 092104.
[8] P. Fischer, A. Züttel, Mater. Sci. Forum 443–444 (2004) 287–290.
[9] S.C. Abrahams, J. Kalnajs, J. Chem. Phys. 22 (1954) 434–436.
[10] G. Renaudin, S. Gomesa, H. Hagemannb, L. Keller, K. Yvon, J. Alloys Compd. 375 (2004) 98–106.
[11] P. Vajeeston, P. Ravindran, A. Kjekshus, H. Fjellvög, J. Alloys Compd. 387 (2005) 97.
[12] G. Lee, J.-Y. Lee, J.S. Kim, Solid State Commun. 139 (2006) 516–521.
[13] L. George, V. Drozd, H. Couvy, J. Chen, S. Saxena, J. Chem. Phys. 131 (2009) 074505–074511.
[14] F. Yu, J.-X. Sun, R.-G. Tian, G.-F. Ji, W.-J. Zhu, Chem. Phys. 362 (2009) 135–139.
[15] B. Sundqvist, O. Andersson, Int. J. Thermophys. 30 (2009) 1118–1129.
[16] A. Corona, M. Marchesi, C. Martini, S. Ridella, Acm. Trans. Math. Software 13 (1987) 262.
[17] A. Tekin, R. Caputo, A. Züttel, Phys. Rev. Lett. 104 (2010) 215501.
[18] R. Caputo, A. Tekin, W. Sikora, A. Züttel, Chem. Phys. Lett. 480 (2009) 203–209.
[19] P. Giannozzi, et al., J. Phys. Condens. Matter 21 (2009) 395502.
[20] S. Clark, M. Segall, C. Pickard, P. Haspin, M. Probert, K. Refson, M. Payne, Z. Krystallogr. 220 (2005) 567.
[21] S. Baroni, S. De Gironcoli, A. Dal Corso, P. Giannozzi, Rev. Mod. Phys. 73 (2001) 515–562.
[22] K. Refson, S. Clark, P. Tulip, Phys. Rev. B. 73 (2006) 155114.
[23] A. Tekin, J.S. Hummelshøj, H.S. Jacobsen, D. Sveinbjörnsson, D. Blanchard, J.K. Nørskov, T. Vegge, Energy Environ. Sci. 3 (2009) 448.
[24] R. Caputo, in: Poster at Impulse Day, PSI November 30, 2007, Villigen, Switzerland.
[25] J. Francisco, I. Williams, J. Phys. Chem. 96 (1992) 7567–7570.
[26] J.-P. Soulie', G. Renaudin, R. Cerny, K. Yvon, J. Alloys Compd. 346 (2002) 200.
[27] R. Caputo, A. Züttel, Mol. Phys. 107 (2009) 1831–1842.
[28] P. Martelli, R. Caputo, A. Remhof, P. Mauron, A. Borgschulte, A. Züttel, J. Phys. Chem. C 114 (2010) 7173–7177.
[29] R. Caputo, F. Guzzetta, A. Angerhofer, Inorg. Chem. 49 (2010) 8756–8762.
[30] R. Caputo, S. Garroni, D. Olid, F. Teixidor, S. Suri nach, M.D. Baró, Phys. Chem. Chem. Phys. 12 (2010) 15093–15100.
[31] R. Caputo, A. Züttel, Mol. Phys. 108 (2010) 1263–1276.
[32] H.L. Johnston, N.C. Hallett, J. Am. Chem. Soc. 75 (1953) 1467–1468.